Title: Growth of β intermetallic in Al-Cu-Si alloy during directional solidification via machine learned 4D quantification

Article Type: Regular article

Corresponding Author: Dr. Biao Cai,

Corresponding Author's Institution: Univerisity of Manchester

First Author: Biao Cai

Order of Authors: Biao Cai; Andrew Kao; Peter D Lee; E Boller; H Basevi; A. B Phillion; A Leonardis; K Pericieous

Abstract: Fe contamination is a serious composition barrier for Al recycling. In Fe-containing Al-Si-Cu alloy, a brittle and plate-shaped β phase forms, degrading the mechanical properties. 4D (3D plus time) synchrotron X-ray tomography was used to observe the directional solidification of Fe-containing Al-Si-Cu alloy. The quantification of the coupled growth of the primary and β phase (Al_5FeSi) via machine learning and particle tracking, demonstrates that the final size of the β intermetallics were strongly influenced by the solute segregation and space available for growth. The temperature gradient direction controlled the β orientation. The work can be used to validate predictive models.
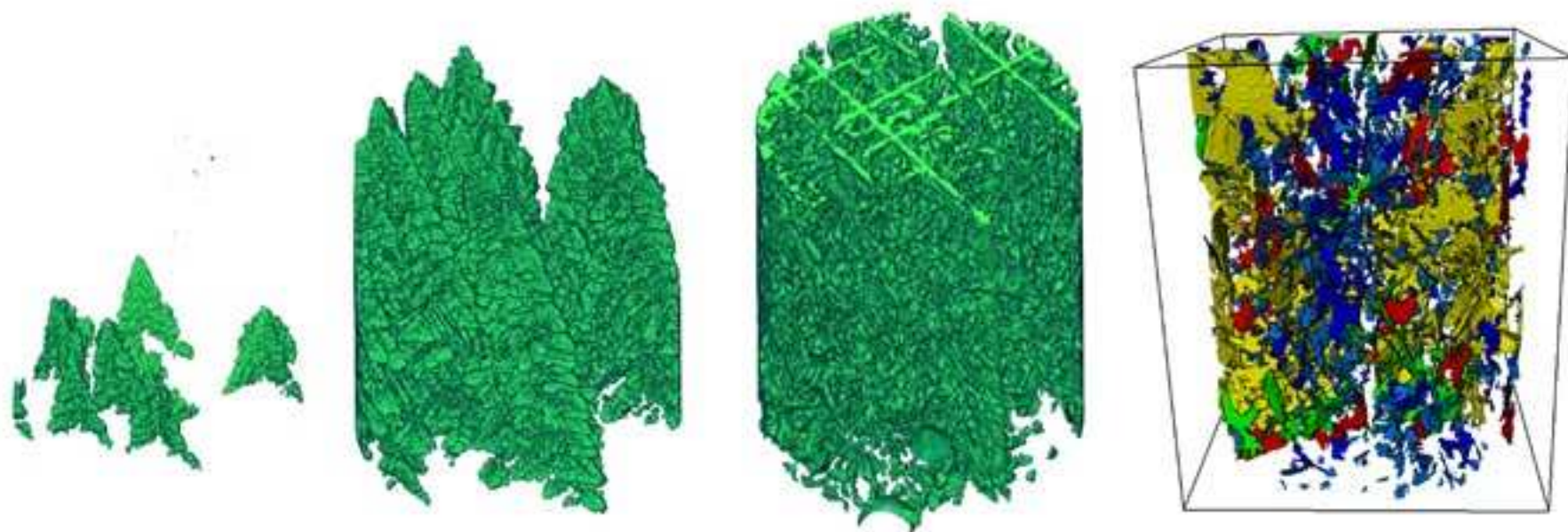
Primary phase

ß intermetallics

Supplementary Material Movie 1

Supplementary Material Movie 2
Click here to download Supplementary Material: SM2.avi

Supplementary Material Movie 3

Growth of β intermetallic in an Al-Cu-Si alloy during directional solidification via machine learned 4D quantification

B.Cai[a,*], A. Kao[b], P.D. Lee[c, **], E. Boller[d], H. Basevi[e], A. B. Phillion[f], A. Leonardis[e], K. Pericleous[b]

[a] *School of Metallurgy and Materials, University of Birmingham, UK;*

[b] *Centre for Numerical Modelling and Process Analysis, University of Greenwich, UK;*

[c] *School of Mechanical Engineering, University College London, UK;*

[d] *ESRF-The European Synchrotron, 71 Avenue des Martyrs, 38000 Grenoble, France;*

[e] *School of Computer Science, University of Birmingham, UK;*

[f] *Dept. of Materials Science and Engineering, McMaster University, Hamilton, Canada*

*b.cai@bham.ac.uk

Growth of β intermetallic in an Al-Si-Cu alloy during directional solidification via machine learned 4D quantification

Fe contamination is a serious composition barrier for Al recycling. In Fe-containing Al-Si-Cu alloy, a brittle and plate-shaped β phase forms, degrading the mechanical properties. 4D (3D plus time) synchrotron X-ray tomography was used to observe the directional solidification of Fe-containing Al-Si-Cu alloy. The quantification of the coupled growth of the primary and β (Al_5FeSi) phase via machine learning and particle tracking, demonstrates that the final size of the β intermetallics were strongly influenced by the solute segregation and space available for growth whereas the β orientation was controlled by the temperature gradient direction. The work can be used to validate predictive models.

Keywords: Al alloys, Intermetallics, Synchrotron X-ray Tomography, 4D Imaging

The full life cycle of aluminium is attractive because recycled aluminium requires as little as 5% of the energy needed for primary production, hence reducing greenhouse emissions [1,2]. However, iron (Fe) continuously accumulates during repeated recycling [3]. As it has low solid solubility in Al, the formation of Fe-rich intermetallic particles during solidification/casting is normally unavoidable [4]. For example, in Al-Si based alloys which have been widely used in engine blocks for automobiles, with the addition of Fe, β phase (Al_5FeSi) can normally form [5–8]. The β phase is plate-shaped and brittle, thereby detrimental to the mechanical properties of the final products[8]. Understanding the nucleation and growth mechanisms of β phase has attracted significant research interest as this knowledge can facilitate the development of innovative and crucially-needed methods to alleviate its unfavourable effects [2].

Solidification of Fe-containing Al alloys has been studied using *in situ* X-ray imaging, providing information on the nucleation and morphological evolution of Fe-containing intermetallics [7,9–14]. Terzi *et al* [10] observed the nucleation of the β phase on the oxide skins and the subsequent growth of the β phase into complex shapes using high

speed X-ray tomography. Puncreobutr *et al* [7] performed a similar experiment with higher temporal resolution. They observed that the nucleation of the β phase was mainly on or near the primary Al dendrites. Additionally, the growth of the β phase is found to be significantly influenced by the primary dendrite arms [7]. Recently, the influence of strontium addition and cooling rates on the intermetallic evolution in Fe-containing Al-10Si alloys was studied by Yu *et al* [11], demonstrating that change of thermal processing conditions and alloy composition could impact the Fe-containing particles. However, none of those studies controlled the thermal field direction; therefore, the growth of intermetallics with regard to the temperature field has not been clearly demonstrated. Moreover, there is litter knowledge regarding to the coupled growth of the primary phase and the intermetallics.

In this study, we aim to illustrate the evolution of β intermetallics during directional solidification of an Al-Si-Cu alloy. High-speed synchrotron X-ray tomography was used to capture the solidification sequence. Detailed quantification of both the primary dendrite and β phase was carried out, providing new insights into the coupled growth of the two phases under a directional temperature field. This result can be used to develop and validate analytical and numerical models for the coupled crystal growth.

The Al-Si-Cu W319 alloy (Al-5.50Si-3.40Cu-0.87Fe-0.27Mg, weight percent) used in this study was provided by Ford Motor Company. A cylinder sample of diameter 1.8 mm was machined by wire-electrical discharge machining. The temperature gradient stage was set up at ID19, European Synchrotron Radiation Facility. The details about the temperature gradient stage, similar to the one in Ref [15] are provided in the supplementary material

 A pink beam with peak energy at 35 keV was used at ID19, ESRF. A high-speed CMOS camera (PCO.DIMAX, Germany) was used for X-ray imaging. The field of

view (FOV) of the camera was set to 2.2 by 2.2 mm and the pixel size is 2.2 µm. The sample was rotated at 2 s per rotation for tomographic data collection. A tomogram with 1000 projections over 180 ° was taken in 1 s and there were 15 s waiting time between two consecutive tomograms for data downloading.

The 319 Al sample was heated up until it was fully molten with a temperature gradient of ~10 °C/mm between the two furnaces (the top furnace was hotter). As the thermocouples were attached to the furnaces, and further away from the sample, the measured temperature was different from the sample temperature. After the sample in the FOV was fully molten, it was held for 15 min. After that, both furnaces were cooled down at the same cooling rate of 0.1 °C/s, which allows the directional growth of the primary phase. As the sample started cooling, high-speed X-ray tomography was started. 47 tomograms were collected and reconstructed by ESRF's reconstruction algorithm with phase retrieval.

Figs. 1a-1f show the vertical cross-section slice at the central plane of the sample as a function of time (supplementary movie S1). The primary phase is dark grey while the liquid is light grey. t_0 is denoted as the time at which the primary phase first appeared in the FOV. The primary phase is observed growing upwards from the bottom of the FOV with a dendritic structure. At $t = t_0 + 224$ s, bright needle-like structures appear within the liquid channels between dendrites (some marked by the arrows in Fig. 1e). These were identified as β intermetallics due to two reasons: (i) they were plate shaped, similar to [7]; and (ii) based on the solidification sequence of W319 alloy (see the supplementary material), the phase formed after the primary phase should be the β intermetallic. Because of its higher Fe content than the melt, it appears much brighter than both the melt and the primary phase in the tomographic slices (e.g. Fig.1e).

With Scheil solidification calculation, the temperature gradient and cooling rate of the sample were then estimated (See the supplement for the procedure). The temperature gradient was estimated to be 6.4 °C/mm and the cooling rate was around 0.078 °C/s, both of which were smaller than the values measured by the thermocouples away from the sample.

We then used Avizo 9.4 (ThermoFisher Scientific) to analyse the 3D images. For the primary phase, a 3D anisotropy diffusion filter followed by an interactive threshold was used. The segmented dendritic structure is shown in Figs.1g-1l and in the supplementary movie S2. Six primary dendrites grew from the bottom of the sample initially, merged into 4 at the later stage of solidification. The dendrites preferred to grow up first at one side of the sample, indicating that macro-segregation of solutes was formed on the other side, inhibiting the growth of primary phase. This indicates that there might be a small horizontal temperature gradient.

Applying a similar procedure to segment the intermetallics turned out to be difficult. To resolve this issue, a machine learning based image processing plugin in ImageJ (Trainable Weka Segmentation [16]) was used. The plugin combines a collection of machine learning algorithms to perform pixel-based segmentations. The detailed procedure for the machine learned segmentation is provided in the supplementary material. This process is fully automated and could be much more timesaving compared to the manual segmentation performed by Puncreobutr *et al* [7].

The 3D shape of the segmented intermetaillic is shown in Fig. 2a to 2d (also see the supplementary video S3). The intermetallics started to form from the bottom of the FOV at t_0+208 s, and grew upwards. Although macro-segregation was observed (Fig. 1h) so that the interface between the primary phase and the liquid was tilted, the β phase grew up with a flat interface indicating that its growth was not largely affected by the

macro-segregation. Another observation is that the intermetallics nucleated from both the sample surface and interior, consistent with Ref. [7].

With the segmented primary and β phase, quantification can then be performed. The volume fraction of the primary phase during solidification is shown in Fig. 3a. It increased linearly at a rate of 0.0016 s^{-1} until it reached around 0.41 at $t=t_0+240$ s. The dendrite growth velocity was measured via tracking the tip position of the dendrite primary arms during solidification. The velocity of four dendrites out of six are shown in Fig. 3b, which have a similar trend. The velocity was highest at the early stage of solidification (~24 μm/s at t_0+32 s), then slowed down to be at around 8 μm/s from t_0+80 s onwards. It is not possible to measure the velocity after the tip reached the top of the FOV at t= t_0+128 s.

Fig. 3a shows the volume fraction of β versus time. The β volume fraction increased almost linearly at a rate of 9.5×10^{-5} s^{-1}. The total number of the β intermetallic and its average volume (total volume of β/total number) against time is shown in Fig. 3c. The total number increased continuously in a linear fashion, as did the average volume. At the end of the experiment (t_0+464 s), 989 intermetallics are found within the FOV. We then measured the volume fraction of intermetallic particles at different heights of the sample. Volumetric data with 30 slices at each chosen height were used for the measurement. As shown in Fig.3d, the curves (β volume fraction as a function of time (t) at different heights (h)) were almost linear with very similar slopes. The intercept of these curves with the x-axis corresponded to the time (t_0) at which β phase just appeared at the chosen height. The   at different heights of the sample is then plotted in Fig.3e. A slope of about 11.7 μm/s was obtained after a linear fitting, which means that the isotherm moved upwards at a speed of 11.7 μm/s as the sample was cooling down. The speed of the isotherm can also be calculated by the ratio of the cooling rate

to the temperature gradient, resulting in a very close value of ~12.2 μm/s. This indicates that our temperature estimation was relatively accurate.

As the sample was cooled down at a constant cooling rate, a linear function between the temperature ($T(h)$) at the sample height (h) and the processing time (t) can be established by Eq. 1:

$$ \tag{1} $$

where   is the β occurrence temperature (595 °C), R is the cooling rate (0.078 °C/s).

Fig.3d can then be re-plotted to β volume fraction versus temperature via eq. 1 (Fig. 3f) along with the Scheil predictions. The experimental result matches well with the Scheil simulation at the early stage of β formation (595 to around 582 °C). However, the prediction and experimental result differ from each other at the later stage of solidification. Similar difference is also reported in [7]. This indicates that although the Scheil model based on equilibrium can predict well the nucleation stage of the intermetallic, it could not make good prediction for the growth stage.

The overall behaviour of β phase with respect to the average volume, total number and volume fraction was linear with decreasing temperature. However, the behaviour of individual β intermetallics remained unclear. To examine this, a particle-tracking algorithm was developed in-house in Matlab (see supplementary material). The volume change (($\qquad\qquad\qquad$, V is the volume) of several individual particles which first appeared at t =t_0+ 240 s is shown in Fig. 4a. The growth dynamics of the intermetallics varied significantly, but most of them grow linearly. We then fitted the curves of the tracked particles' volume vs time with linear functions. The slopes are the volume growth rate of the β intermetallics. Fig. 4b shows the histogram of the volume growth rate of the intermetallics on a log x-axis, which shows a normal distribution. The intermetallics were then separated and coloured based on the volume growth rate as

shown in Fig. 4c (green – intermetallics with velocity less than 7, 000 μm^3/s whereas purple – more than 7, 000 μm^3/s). 7, 000 μm^3/s was chosen based on the histogram (Fig. 4b). The particles with higher velocity have the following characteristics: (1) connected to the sample outer surface (Fig. 4c); (2) located within the regions where macro-segregation was observed and/or within primary dendrite arms (Fig. 4d); and (3) they were connected particles (several particles grew together into a single one). The particles with smaller volume growth rates distributed more homogeneously across the sample (Fig. 4c) and the majority of the particles with a lower growth rate were located within the sample interior. A closer look at those particles shows that they were mostly within secondary dendrite arms (Fig. 4e). The variation of the growth velocity indicates that the growth of β particles was influenced by the local environment they experienced (e.g. composition variation due to micro and macro segregation, and the space available for growth). If an β intermetallic nucleated in the region with macro-segregation, it had abundant solutes and liquid space for growth hence it grew large. If the β phase nucleated in the region within the secondary dendrite arms, its growth would be much more restricted. This finding can have implications for modelling intermetallic growth in casted components [17,18] – the size and growth rate of the intermetallics are directly related to the macro segregation behaviour of the casted components.

We then used an ImageJ plugin-BoneJ [19] to measure the local thickness of the intermetallics, defined as the diameter of the greatest sphere that can fit within the structure. The 3D rendering of the local thickness is shown in Fig. 2e and 2f. Fig. 4d shows the mean local thickness and its standard deviation against time. It increased from 8 to only 11 μm during solidification. The mean local thickness at $t=t_0+464$ s is 11 μm with a standard deviation of 4 μm. The maximum is about 20 μm. The reluctant increase of local thickness was also observed by [7].

To determine the orientation of those particles, we used principal component analysis (PCA) as described in [7,20]. Assuming the β phase was plate-shaped, the 3rd component of PCA analysis shall be the normal direction of the plates. The angle (θ) between the 3rd component and the vertical direction (Z) of the tomographic volume should determine the orientation of the intermetallics with respect to the temperature field direction (Z). However, for intermetallics complicated in geometry with holes and branches and/or connected with others (Fig.4e), θ value derived from PCA may not correctly measure their orientations. To remove those particles from the θ calculation, an empirical method was applied - particles with plate thickness (module of the 3rd PCA component) larger than 20 μm were not used for the orientation calculation. This value was chosen according to the BoneJ measurement that the maximum local thickness was ~20 μm. Fig. 4h shows the polar histogram of the angle θ at two time steps. The θ angle was distributed mainly within 60 to 120°, and peaked at around 90 °. This shows that most of the β phase was oriented almost parallel to the Z direction, which indicates that the growth direction of the β phase was strongly influenced by the heat flow induced by the directional temperature gradient.

In summary, 4D synchrotron X-ray tomography was used to study directional solidification of a Fe-containing W319 Al alloy. The work shows that the overall growth of the primary and β phase was linear as a function of time/temperature when the sample was cooling down at a constant cooling rate of 0.078 °C/s under a temperature gradient of 6.4 °C/mm. During solidification, a macro-segregation zone formed on one side of the sample. The growth rate of the β intermetallics were largely determined by the interdendritic space available for growth. The intermetallics nucleated in the macro-segregation zone as well as some large inter-primary dendritic liquid regions had abundant space to grow hence grew quickly to large crystals. The

intermetallics nucleated between the secondary dendrite arms were restricted and grew slower. The heat flow direction influenced the orientation of β intermetallics, so that the normal vector of the plate-shape intermetallics was perpendicular to the heat flow direction.

References

[1]   John A. S. Green, Aluminum Recycling and Processing, ASM International, 2007.

[2]   C.B. Basak, N.H. Babu, Sci. Rep. 7 (2017) 1–10.

[3]   L. Zhang, J. Gao, L.N.W. Damoah, D.G. Robertson, Miner. Process. Extr. Metall. Rev. 33 (2012) 99–157.

[4]   T.O. Mbuya, B.O. Odera, S.P. Ng'ang'a, Int. J. Cast Met. Res. 16 (2003) 451–465.

[5]   T. Smith, K. O'Reilly, S. Kumar, I. Stone, Metall. Mater. Trans. A Phys. Metall. Mater. Sci. 44 (2013) 4866–4871.

[6]   C.B. Basak, N. Hari Babu, Mater. Des. 108 (2016) 277–288.

[7]   C. Puncreobutr, A.B. Phillion, J.L. Fife, P. Rockett, A.P. Horsfield, P.D. Lee, Acta Mater. 79 (2014) 292–303.

[8]   L.A. Narayanan, F.H. Samuel, J.E. Gruzleski, Met. Mat. Trans. A 25 (1994) 1761–1773.

[9]   J. Wang, P.D. Lee, R.W. Hamilton, M. Li, J. Allison, Scr. Mater. 60 (2009) 516–519.

[10]   S. Terzi, J.A. Taylor, Y.H. Cho, L. Salvo, M. Suéry, E. Boller, A.K. Dahle, Acta Mater. 58 (2010) 5370–5380.

[11]   J.M. Yu, N. Wanderka, A. Rack, R. Daudin, E. Boller, H. Markötter, A. Manzoni, F. Vogel, T. Arlt, I. Manke, J. Banhart, J. Alloys Compd. 766 (2018) 818–827.

[12]   B. Kim, S. Lee, S. Lee, H. Yasuda, Mater. Trans. 53 (2012) 374–379.

[13]   S. Feng, E. Liotti, A. Lui, S. Kumar, A. Mahadevegowda, K.A.Q.O. Reilly, P.S. Grant, Scr. Mater. 149 (2018) 44–48.

[14]   A. Bjurenstedt, D. Casari, S. Seifeddine, R.H. Mathiesen, A.K. Dahle, Acta Mater. 130 (2017) 1–9.

[15]   B. Cai, J. Wang, A. Kao, K. Pericleous, A.B. Phillion, R.C. Atwood, P.D. Lee, Acta Mater. 117 (2016) 160–169.

[16]   I. Arganda-Carreras, V. Kaynig, C. Rueden, K.W. Eliceiri, J. Schindelin, A. Cardona, H.S. Seung, Bioinformatics 33 (2017) 2424–2426.

[17]   J. Wang, M. Li, J. Allison, P.D. Lee, J. Appl. Phys. 107 (2010) 1–8.

[18]   J. Allison, M. Li, C. Wolverton, X.M. Su, Jom 58 (2006) 28–35.

[19]   M. Doube, M.M. Kłosowski, I. Arganda-Carreras, F.P. Cordelières, R.P. Dougherty, J.S. Jackson, B. Schmid, J.R. Hutchinson, S.J. Shefelbine, Bone 47 (2010) 1076–1079.

[20]   S. Yue, P.D. Lee, G. Poologasundarampillai, J.R. Jones, Acta Biomater. 7 (2011) 2637–2643.

Fig 1. (a to e) 2D longitudinal cross-sectioned slices, and (f to j) 3D rendering of the segmented primary phase: (a) and (f) at t_0; (b) and (g) at t_0+36 s; (c) and (h) at t_0+80 s; (d) and (i) at t_0+160 s; (e) and (j) at t_0+464 s (scale bar: 300 µm).

Fig 2. (a) An original greyscale slice at the height of 440 µm at t0+464 s; (b) red colour showing regions segmented for the β phase via the interactive method; (c) probability map of the β after wika trainable segmentation; (d) the segmented β intermetallics (black needles); (e) and (f) the enlarged view of the original greyscale slice and the corresponding segmented β phase (black needles in the image) (scale bar: 300 µm).

Fig 3. (a) to (d) volume rendering of β intermetallics, at t_0+ (a) 224 s; (b) 288 s; (c) 352 s; and (d) 464 s; (e) and (f) the distribution of local thickness of the β intermetallics at t_0+(e) 352 s; and (f) 464 s. (scale bar: 300 µm).

Fig 4. Quantification of individual β intermetallics: (a) the volume change of particles appearing from t =t0+ 240 s; (b)the histogram of the volume velocity of β particles on a log x-axis; (c) β particles in 3D at t =t0+ 464 s color-coded by their velocity (low velocity - green< 7000 um3/s, high velocity - purple > 7000 um3/s); (d) β particles (purple) with high velocity at t =t0+ 464 s and the primary phase (blue) at t =t0+ 128 s; (e) a region of interests showing β particles with low velocity (green) and primary phase (blue) at t =t0+ 464 s; (f) the average local thickness vs time; (g) a connected β particle; and (h) rose histogram of angle θ.
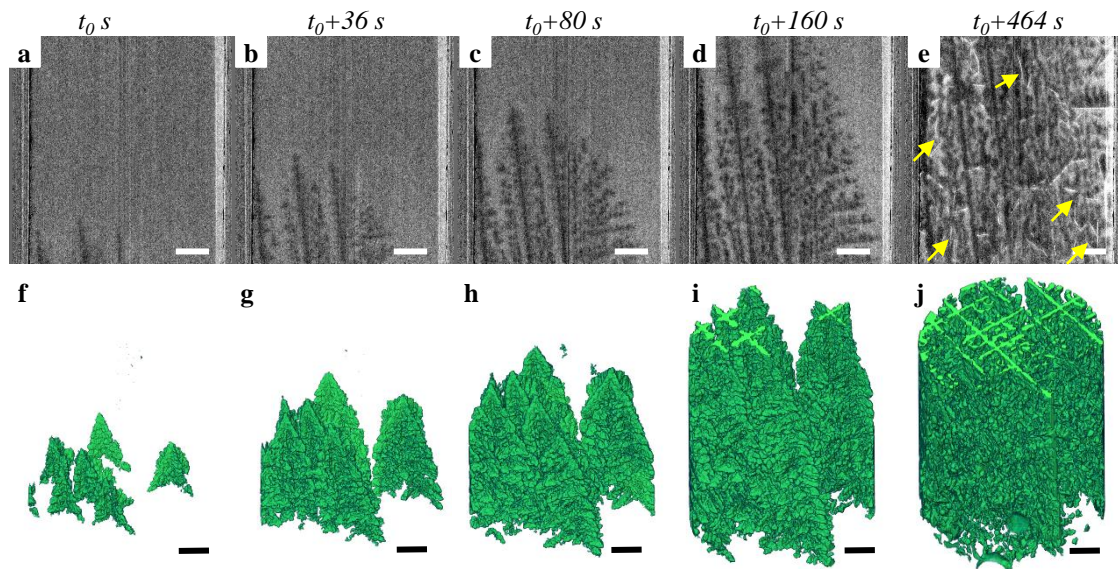
Figure(s)

Fig.1. (a to e) 2D longitudinal cross-sectioned slices from the 4D tomography, and (f to j) 3D rendering of the segmented dendritic primary phase: (a) and (f) at t_0; (b) and (g) at t_0+36 s; (c) and (h) at t_0+80 s; (d) and (i) at t_0+160 s; (e) and (j) at t_0+464 s (scale bar: 300 µm).
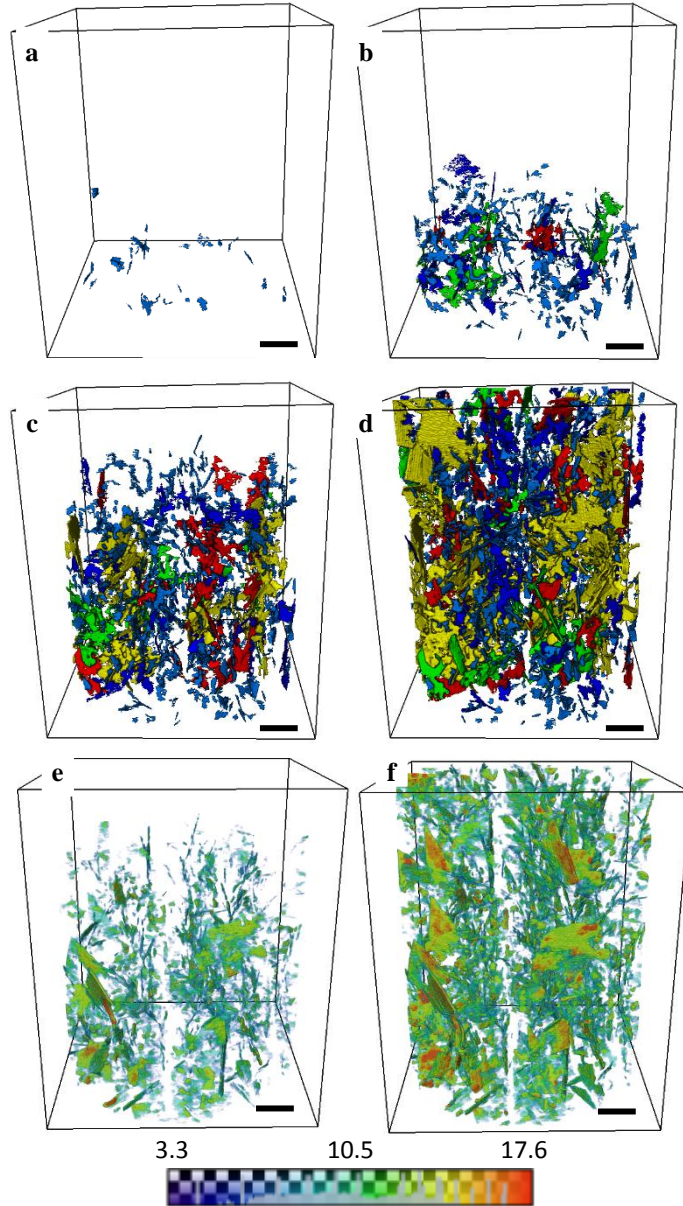
3.3   10.5   17.6

Fig.2. (a) to (d) volume rendering of β intermetallics, at $t= t_0 +$ (a) 224 s; (b) 288 s; (c) 352 s; and (d) 464 s; (e) and (f) the distribution of local thickness of the β intermetallics at (e) 352 s; and (f) 464 s. (scale bar: 300 μm).
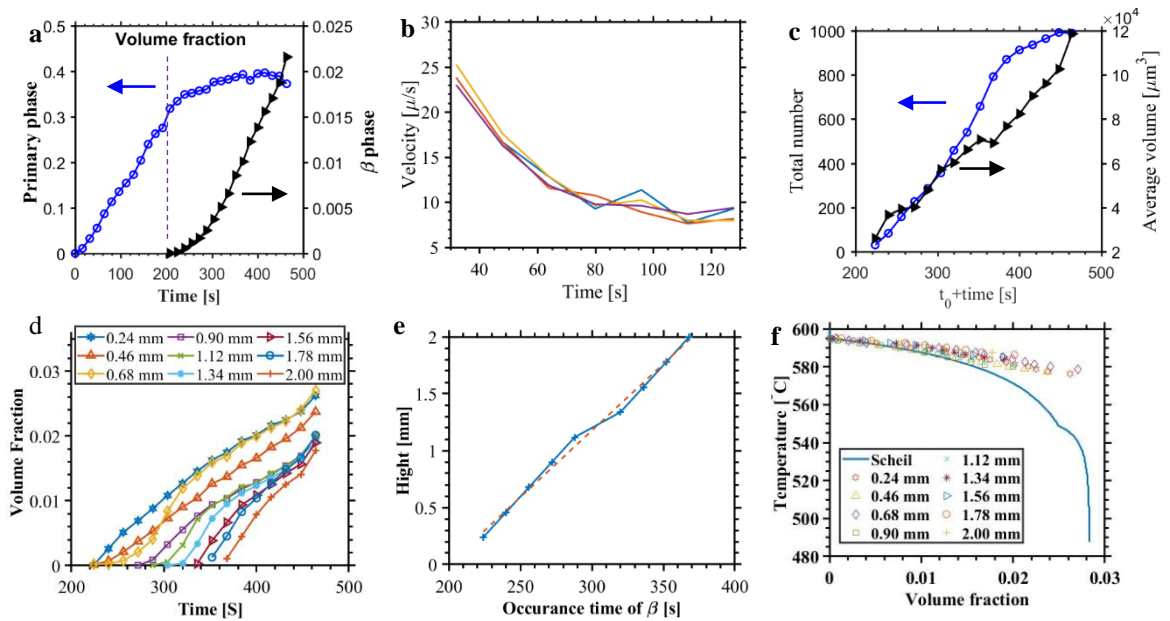
Fig.3. Quantification of the primary and β phase: (a) volume fraction of primary and β phase; (b) the velocity of primary dendrite arm growth; (c) total number and average volume of β particles; (d) volume fraction of β phase at different height of the sample; (e) the first observation of β phase at different heights; and (f) volume fraction of β phase as a function of temperature calculated by Scheil model and tomographic analysis.
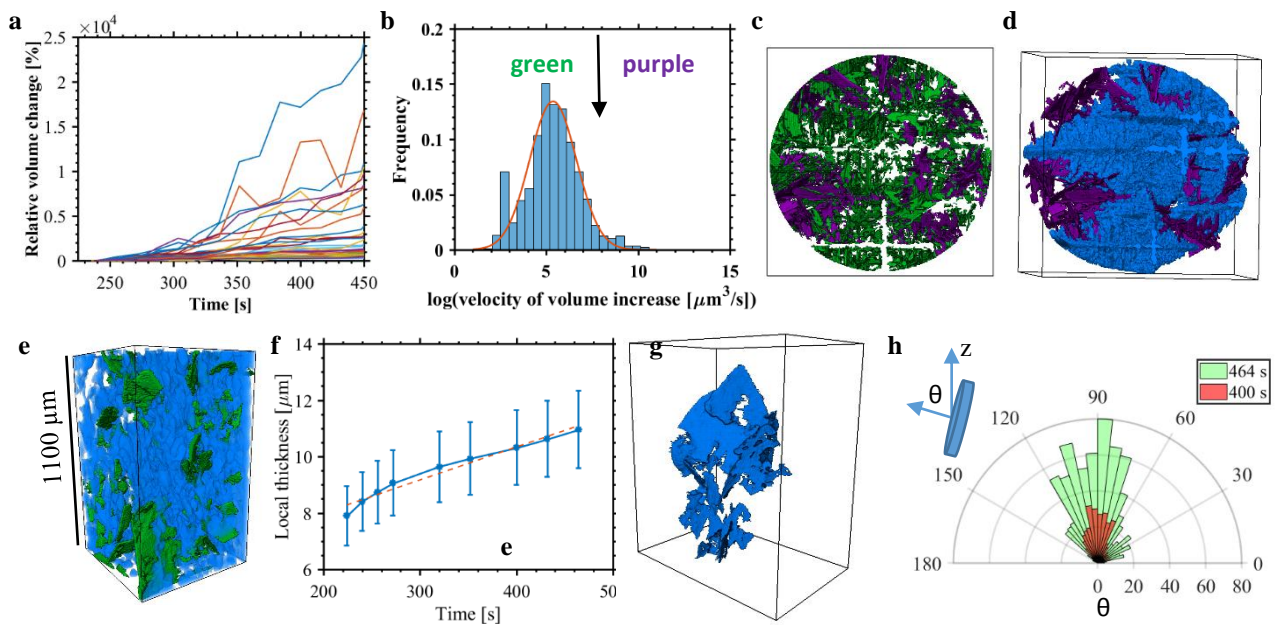
Fig.4. Quantification of individual β intermetallics: (a) the volume change of individual particles appearing from $t = t_0 + 240$ s; (b)the histogram of the volume velocity of β particles on a log x-axis; (c) β particles in 3D at $t = t_0 + 464$ s color-coded by their velocity (low velocity - green< 7000 um³/s, high velocity - purple > 7000 um³/s); (d) β particles (purple) with high velocity at $t = t_0 + 464$ s and the primary phase (blue) at $t = t_0 + 128$ s; (e) a region of interests showing β particles with low velocity (green) and primary phase (blue) at $t = t_0 + 464$ s; (f) the average local thickness vs time; (g) a connected β particle; and (h) rose histogram of θ - angle between the 3rd component of principle component analysis and the vertical direction (Z) of the tomographic volume.

Supplementary Material

Click here to download Supplementary Material: Supplementary.docx